Journal of Molecular Graphics and Modelling 27 (2008) 255–265

Contents lists available at ScienceDirect

Journal of Molecular Graphics and Modelling

journal homepage: www.elsevier.com/locate/JMGM

Radial scan of the molecular electrostatic potential of RNA double helices: An application to the enzyme-tRNA recognition

Ray M. Marín, William A. Agudelo, Edgar E. Daza C. *

Grupo de Química Teórica, Universidad Nacional de Colombia and CeiBa, Bogotá D.C., Colombia

ARTICLE INFO

Article history:
Received 17 December 2007
Received in revised form 28 April 2008
Accepted 29 April 2008
Available online 4 May 2008

Keywords:
Molecular electrostatic potential
Electrostatic complementarity
Molecular recognition
Protein–RNA interactions
Aminoacylation activity

ABSTRACT

We introduced a method to characterize quantitatively the molecular electrostatic potential (MEP) of the minor and major grooves of base pairs located at nucleic acid double helices. By means of a radial MEP scan, we obtained a *n*-tuple of potential values corresponding to each groove, which can be analyzed by plotting the MEP values as a function of the angle in the radial scan. We studied base pairs of two different tRNAs, relevant in the recognition process with their cognate aminoacyl tRNA synthetases (aaRSs), in order to correlate their electrostatic behavior with the corresponding aminoacylation activity. We analyzed the first three base pairs of the *Escherichia coli* $tRNA^{Ala}$ acceptor stem, finding several cases where the MEP profiles obtained from the plots are in agreement with the reported aminoacylation activities. Additionally, a non-hierarchical clustering performed over the MEP *n*-tuples resulted in meaningful classifications that correlate with the activity and with the predicted stereochemistry of the reaction. We also studied the first two base pairs of the *E. coli* $tRNA^{Thr}$ acceptor stem but constraining the analysis to the angle intervals that seem relevant for the binding sites of the enzyme. These intervals were deduced from the ThrRS-$tRNA^{Thr}$ complex crystal structure. In this case, we also found a good agreement between the MEP profiles and the activity, supporting the idea that the tRNA identity elements function is to allow an optimal electrostatic complementarity between the aminoacyl-tRNA synthetase and the tRNA.

1. Introduction

Protein–nucleic acid interactions play a central role in many biological processes of living systems. One of such processes is the aminoacylation reaction where the aminoacyl-tRNA synthetase (aaRS) joins each tRNA with its cognate amino acid. In this reaction, that translates the nucleic acids language into the proteins language, the fidelity of the translation is fundamental to obtain functional proteins. This fidelity is guaranteed by the highly specific recognition between aaRS and tRNA. During the last three decades, considerable effort has been made to understand the basis of this specificity by means of aminoacylation assays *in vivo* and *in vitro* [1]. From the wide variety of results, the main conclusion is that each tRNA has a proper set of nucleotides, mainly located in the anticodon arm and in the acceptor stem, that are responsible for the correct recognition by the enzyme and in consequence they have been called *identity elements* [2].

The identity elements are nucleotides that must be present in certain positions of each tRNA sequence to allow the recognition by the enzyme. For assays *in vitro*, if one of these nucleotides is changed by another, the aminoacylation activity (measured as k_{cat}/K_M) is reduced dramatically [2]. Although these identity elements can be found after several aminoacylation assays, there is not a theory capable of predicting them. It is only with the advances in computational chemistry that some theoretical studies have lead to get insights into the molecular basis of aaRS-tRNA interaction and in some cases, about the identity elements effect on molecular recognition. The work by Tworowski and Safro [3,4] shows that for several aminoacylation systems the primary non-specific recognition between aaRS and tRNA is due to long range electrostatic interactions, consequence of the attraction between the predominantly negative electrostatic potential around tRNA and the areas of positive potential around the enzyme. When the results of the electrostatic calculations for several aaRSs are compared with the corresponding 3D representations of the complex aaRS-tRNA, it is evident that the positive potential is generated at the tRNA binding sites of the protein and independently of whether the enzymatic complexes are monomeric, dimeric or heterotetrameric, there is always one "positive area" for each one of those binding sites. On the other hand,

* Corresponding author.
E-mail addresses: rmmarinf@unal.edu.co (R.M. Marín), waagudelos@unal.edu.co (W.A. Agudelo), eedazac@unal.edu.co (E.E. Daza C.).

1093-3263/$ – see front matter © 2008 Elsevier Inc. All rights reserved.
doi:10.1016/j.jmgm.2008.04.011

Beuning and co-workers were trying to identify atomic groups governing the molecular recognition on the 2–71 base pairs of the *Escherichia coli* $tRNA^{Ala}$ (this position is an identity element) [5]. Although they were not able to find them, they showed for eight base pairs that similarity of the electrostatic potential in the major groove was reflected in the aminoacylation activity, i.e., electrostatically similar base pairs had similar activities.

These findings agree with the notion of *electrostatic complementarity* or the *electrostatic lock*, as it was previously proposed by Náray-Szabó[6–9]. He proposed that a more complete key-and-lock model to recreate enzyme–substrate interaction has to consider the electrostatic fit as well as the geometrical fit, since the enzyme has to find its electrostatic counterpart in the binding site in order to allow maximum interaction between molecules. Several works based on this idea showed that a better biological recognition is obtained when a better electrostatic complementarity is reached [6–15].

Encouraged by this findings, our purpose is to study the electrostatic behavior of different base pairs known as identity positions in the *E. coli* $tRNA^{Ala}$ and $tRNA^{Thr}$ acceptor stems, to show that the molecular electrostatic potential (MEP) generated by these pairs of nucleotides determines the "shape of the key" that must fit in the "electrostatic lock" of the corresponding aaRS. In the present work, we considered the base pairs in positions 1–72, 2–71 and 3–70 for $tRNA^{Ala}$ [5,16–25] and 1–72 and 2–71 for $tRNA^{Thr}$ [26,27].

Since the geometry of the AlaRS-$tRNA^{Ala}$ complex has not been obtained yet, we cannot study the protein-tRNA interactions in a direct way. However, as all aminoacylation activities were obtained with the same enzyme (*E. coli* AlaRS) we expect that base pairs with similar MEP will have similar electrostatic complementarity with the enzyme, and therefore they will induce similar activities, as has been suggested by Náray-Szabó [8,9]. Additionally, since the AlaRS-$tRNA^{Ala}$ interactions are expected to be similar to those observed in the ThrRS-$tRNA^{Thr}$ complex [28], specially in the interaction involving the acceptor stem, we assume that performing the same analysis over this second system would serve as a guide to evaluate the results obtained for the alanine system. Since the ThrRS-$tRNA^{Thr}$ crystal structure for *E. coli* is known [27], in this case we are able to identify the binding sites of the enzyme close to the first two base pairs of the acceptor stem and, therefore, we can compare the MEP in the involved region in order to test our hypothesis, i.e. to corroborate if there is a correlation between the MEP in such region and the activity. This electrostatic characterization might be considered as new evidence to establish the molecular basis of the identity elements function in the aaRS-tRNA recognition process.

For a quantitative comparison of MEPs generated in the surroundings of each base pair, we need to evaluate the MEP field in some particular regions. We have chosen separately the zones of the minor and major grooves, where the atoms of the bases are more exposed to the enzyme. By means of a *radial MEP scan*, the MEP associated with each base pair in the minor and major grooves can be characterized by *n*-tuples of MEP values, e.g. one *n*-tuple of MEP values for each groove. As the *n*-tuples are suitable to be plotted as *V* versus the scan angle, comparisons may be performed graphically or quantitatively using the Euclidean distance. The analysis of the plots revealed several cases where the MEP profiles correlate with the corresponding activity of the base pair, in both the $tRNA^{Ala}$ and the $tRNA^{Thr}$. Additionally, non-hierarchical clustering analysis performed over the distance matrices for the $tRNA^{Ala}$ base pairs, produced simple classifications that agreed with the aminoacylation activity and with the predicted stereochemistry of the AlaRS-$tRNA^{Ala}$ interaction.

2. Methodology

2.1. Modeling the $tRNA^{Ala}$ acceptor stem

In Fig. 1, we show the localization of the first three base pairs in the tRNA acceptor stem and the kind of molecular fragments used to model each position. The fragments used to model the first pair are constituted by five nucleotides, while the fragments for the second and third pairs are made of six. We chose these fragments including the first neighbors of the base pair, as they are in the complete tRNA, in order to include the stereochemistry of double helices and the steric and stacking effects induced on the base pair of interest. The neighbor nucleotides remain constant and correspond to the wild-type sequence of the corresponding tRNA. In Table 1 are the pairs considered in each position for the $tRNA^{Ala}$ and $tRNA^{Thr}$ acceptor stems, ordered according to their corresponding aminoacylation activities. The original activity values are normalized to the wild-type pair which always has $k_{cat}/K_M = 1.0$. However, here we prefer to use the $-\log K = -\log k_{cat}/K_M$ values which facilitate the interpretation of the final results. It is worth

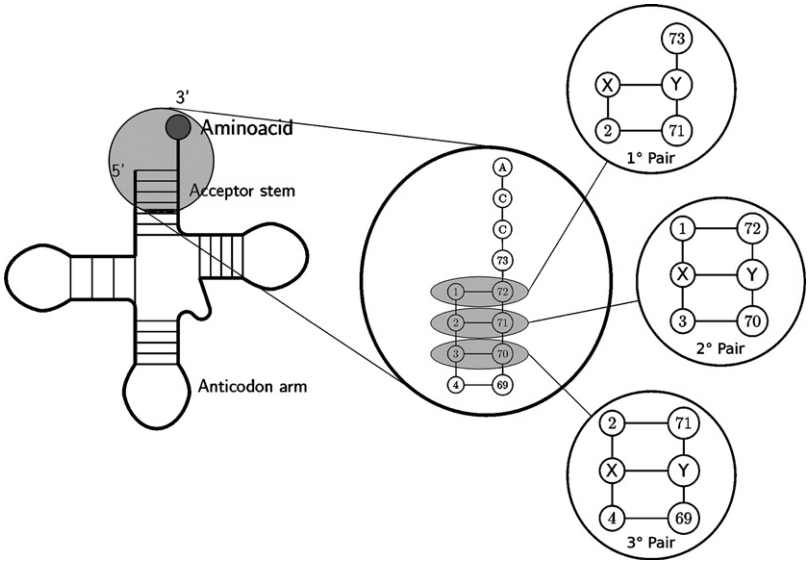

Fig. 1. Double helix RNA fragments built to model the base pairs X–Y in the $tRNA^{Ala}$ and $tRNA^{Thr}$ acceptor stems.

Table 1
Aminoacylation activities in descendant order for the X–Y base pairs tried out in each position

$tRNA^{Ala}$ variants								
Pairs 1–72 [a]			Pairs 2–71 [b]			Pairs 3–70 [c]		
No.	X–Y	$-\log K$ [d]	No.	X–Y	$-\log K$	No.	X–Y	$-\log K$ [e]
1	G-C [f]	0.000	1	G-C [f]	0.000	1	G-U [f]	0.000
2	7DAG-C	−0.322	2	I-C	0.292	2	2AA-IsoC	0.398
3	I-C	0.174	3	G-4HC	0.602	3	G-dU	1.252
4	G-4HC	0.469	4	2AA-U	0.638	4	I-U	2.432
5	U-2AP	1.260	5	2AP-U	0.745	5	A-U	3.046
6	2AP-U	1.886	6	7DAG-C	1.420	6	U-G	3.046
7	C-7DAG	2.201	7	7DAG-4HC	1.658	7	G-C	4.000
8	A-U	2.398	8	U-2AA	1.699			
9	U-A	2.398	9	U-A	1.921			
10	C-I	2.620	10	A-U	1.959			
11	4HC-G	2.620	11	U-2AP	4.000			
12	C-G	4.000	12	C-I	4.000			
			13	C-G	4.000			

$tRNA^{Thr}$ variants					
Pairs 1–72 [g]			Pairs 2–71 [g]		
No.	X–Y	$-\log K$	No.	X–Y	$-\log K$
1	G-C [f]	0.000	1	C-G [f]	0.000
2	A-U	1.921	2	U-A	2.222
3	C-G	2.699	3	G-C	2.745
			4	A-U	3.602

[a] Ref. [24].
[b] Ref. [5].
[c] Ref. [25].
[d] In this expression, $K = k_{cat}/K_M$. In cases, where $k_{cat}/K_M = 0$, we have taken $K = 0.0001$ in order to avoid the indetermination of $\log(0)$.
[e] For this pair, in the original reference they report the $\Delta\Delta G^{\ddagger} = -RT \ln(k_{cat}/K_M)$ values in kcal/mol. The number shown here was calculated considering $R = 0.00198$ kcal/mol K and $T = 298$ K according with the authors [19,29].
[f] Base pair present in the wild-type sequence.
[g] Ref. [26].

noting that experimental results for $tRNA^{Ala}$ are obtained from $duplex^{Ala}$ [5,24] or $microhelix^{Ala}$[5,25] that resemble the $tRNA^{Ala}$ acceptor stem and that have shown to retain the same specificity in *in vitro* assays as the whole tRNA.

The nuclear geometries for the RNA fragments were built considering the *A* 3′ *endo* conformation, with standard angles and distances for the Watson–Crick base pairs, i.e. pairs in positions 1–72 and 2–71 in $tRNA^{Ala}$ and $tRNA^{Thr}$ acceptor stems. In these cases, the sugar-phosphate backbone was optimized using molecular mechanics with the AMBER [30] force field and a cutoff value for the energy change of 0.05 kcal/Å mol. The geometries for the base pairs in positions 3–70 of the $tRNA^{Ala}$ were obtained as a snapshot from the molecular dynamics study performed by Nagan et al. [25]. It is worth noting that in all cases the obtained geometries agreed with the hydrogen bonding pattern reported for those pairs (see Fig. 2).

In order to find out which regions of the minor or major groove of the $tRNA^{Thr}$ acceptor stem are in close interaction with the enzyme atoms, we search in the PDB file of the *E. coli* ThrRS-$tRNA^{Thr}$ complex, deposited in the Protein Data Bank with the code: 1QF6 [31].

2.2. Stereochemical considerations about the minor and major groove

Before we show our results, it is necessary to recall that both DNA and RNA double helices, present two well characterized domains: the minor and major grooves. In Fig. 3 (a) and (b), we illustrate the two grooves using the MEP calculated over the solvent accessible surface for a GC–GC–GC double helix fragment. Since AlaRS and ThrRS are class II enzymes, they are expected to approach to the acceptor stem toward the major groove, however, it has been previously found that these two enzymes also interact with the minor groove, being a particular case in the class II enzymes. For each one of the first three base pairs of the $tRNA^{Ala}$ acceptor stem, it has been previously established that the AlaRS should recognize the major groove in the 1–72 [22,24] and 2–71 [5] pairs and the minor groove in the 3–70 pair [19,21]. From the geometry of the ThrRS-$tRNA^{Thr}$ complex it has been established that the enzyme has hydrogen bond interactions with atoms in the minor groove of $tRNA^{Thr}$ acceptor stem: the Tyr205 with the G1-C72 base pair and the Gly203 with the C2-G71 base pair [27]. Thus, these apparent stereochemical preferences of the enzymes must be taken into account in the search of meaningful similarities among base pair MEPs, so we must be able to study each groove separately to avoid confusions in the interpretation of the final conclusions.

2.3. The radial MEP scan

Molecular electrostatic potential characterization is a complex problem; a brute force approach to solve this problem may be, for instance, to compare these scalar fields associated to each molecule point by point using an high resolution grid. The main problem of this approach is that it would require to test a huge number of possible orientations of the molecules, in such a way that the similarity would be maximized. This approach is clearly infeasible. Another possibility is to make visual comparisons, but they are also limited [32]. This implies that it is imperative to find alternative representation schemes that reduce the search space, preserving the really important information.

Algorithmic procedures to measure similarity can be classified as "alignment dependent (AD)" or "alignment independent (AI)" if the superposition of molecular frames is required or not (see Ref.

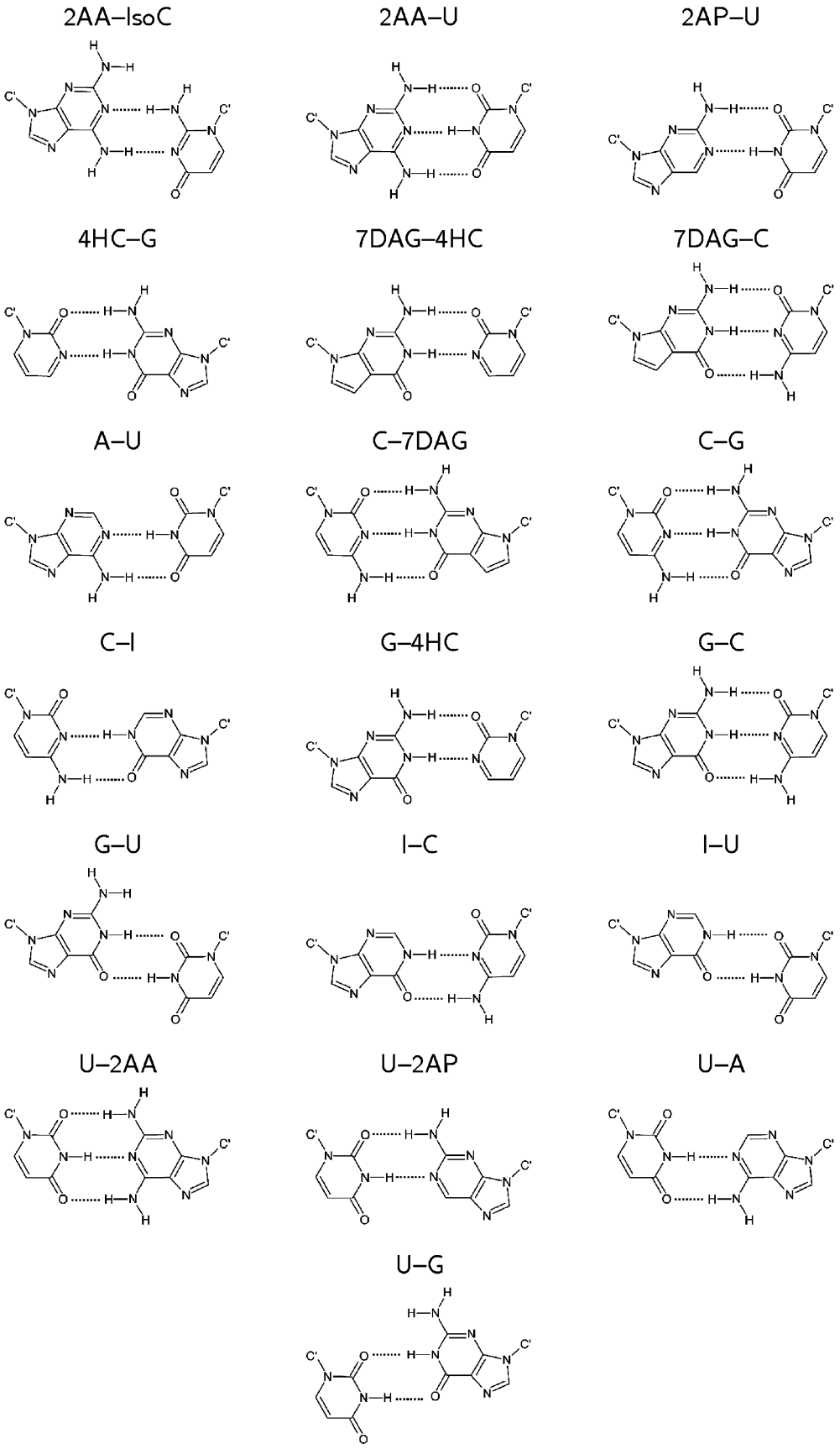

Fig. 2. Hydrogen bonding patterns for the studied base pairs. Taken from Refs. [5,24,25].

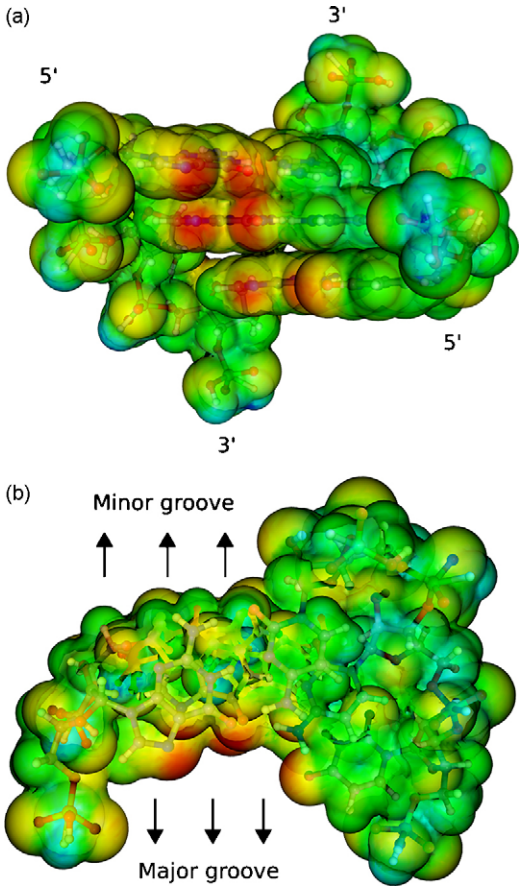

Fig. 3. MEP on the solvent accessible surface for a GC–GC–GC double helix fragment. In (a) we show the $5' \rightarrow 3'$ direction of sugar-phosphate backbones. In (b) the same fragment is shown from an upper view and the minor and major grooves can be identified as the wider and narrower ones respectively. Images obtained with Molekel 5.1.

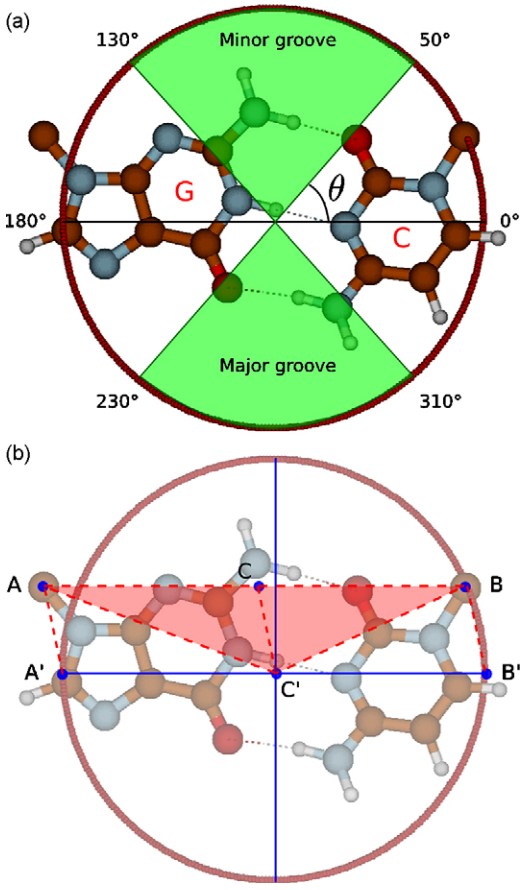

Fig. 4. (a) The base pair is centered in a circumference to carry out the radial scan. In green, we show the representative intervals of the minor ($50^\circ \leq \theta \leq 130^\circ$) and major grooves ($230^\circ \leq \theta \leq 310^\circ$) of the tRNA fragments. (b) Circumference building process: the two sugar carbon atoms joined to the nitrogenated bases are located (points A and B). The middle point of the *AB* line (*C*) and the centroid of the bases atoms (*C*′) are calculated. The *A* and *B* points are moved according to the *n*-tuple *CC*′ generating the *A*′*B*′ line. Finally, the circumference centered at *C*′ with radius $|B' - C'|$, on the *ABC*′ plane is generated.

[33] and references therein). Following the AD philosophy, here we propose a simple choice of points to calculate and compare the MEP. Based on the symmetry of the base pairs, we calculate the potential over a circumference defined on the horizontal plane defined by the nitrogenated base pair, in such a way that we can monitor the electrostatic behavior of the base pair surroundings, i.e. a radial MEP scan. By controlling the angle interval covered in the scan, we can separate the minor groove from the major groove (see Fig. 4 (a)). In that figure it is possible to see that the circumference crosses both grooves at similar distances from the nuclei, i.e. the base pair is circumscribed in the circumference.

To obtain comparable data, equivalent structural regions must be compared, therefore three conditions need to be fulfilled: (i) the radius of the circumference must be very similar for all cases, (ii) the base pair must be circumscribed in the circumference and (iii) the circumference plane must describe the hypothetical horizontal plane of the base pair. In the following, we will describe the building process in detail.

In order to keep an almost constant radius, we took half of the distance between the sugar carbon atoms joined to the nitrogenated bases, since it is well know that it is a very conserved distance among the studied base pairs [34,35]. In Fig. 4(b), these carbon atoms correspond to the points *A* and *B*. Once these two points are identified, we obtain the middle point *C* of the *AB* segment and the centroid *C*′ of the nuclear coordinates of the atoms in the base pair, i.e. the point calculated from:

$$\begin{aligned} x_{C'} &= \frac{\sum_i^n x_i}{n} \\ y_{C'} &= \frac{\sum_i^n y_i}{n} \\ z_{C'} &= \frac{\sum_i^n z_i}{n}, \end{aligned} \tag{1}$$

where *n* is the total number of atoms in the two bases. This centroid *C*′ will be the center of the circumference. Points *A*, *B* and *C*′ define the plane of the circumference. Points *A*′ and *B*′ are generated by mapping the *AB* segment in such a way that *C* coincide with *C*′. Accordingly, the point where the angle θ (theta) is 0° is defined by the segment *C*′*B*′ (see Fig. 4(b)). In this way, the circumference is generated by all the points on the *ABC*′ plane that are at a distance *d* from *C*′:

$$d = \frac{|B - A|}{2} = \frac{|B' - A'|}{2} = |B' - C'|. \tag{2}$$

Once the circumference is defined, the MEP can be calculated at any of its points. In this paper, we have used an *ab initio* molecular

electrostatic potential, which is calculated according to:

$$V(r) = \sum_i^N \frac{Z_i}{|R_i - r|} - \int \frac{\rho(r')\,dr'}{|r' - r|}, \quad (3)$$

where the first term at right is the potential due to the nuclei and the second one is the potential due to the electron cloud represented by the electronic density function $\rho(r')$ obtained from standard electronic wave function calculations. In this case, the quantum mechanical calculations were performed at HF/6-31G level [36].

The MEP for each base pair was calculated on the circumference every 1° (one degree) to obtain a *n*-tuple:

$$\mathbf{V} = (V_{1^\circ}, V_{2^\circ}, \ldots, V_{360^\circ}) \quad (4)$$

Since our interest is on the atoms of the bases that are exposed in each groove, we just need one circumference by base pair in order to characterize their surroundings. This is the main advantage of our approach, in as much as we employ only one *n*-tuple by pair, we avoid to lose some details that might be obscured by considering explicitly the information of the neighbor pairs.

Although the base pairs are not necessarily coplanar, i.e. nitrogenated bases may be oriented in such a way that their planes do not coincide, the plane we have defined turns out to be an "average" plane. In Fig. 5, we show the base pairs studied in the third pair of the tRNA corresponding to Ala with their corresponding circumferences. In the upper view, it is possible to observe that the circumferences actually cover the minor and major groove regions where the most exposed atoms could establish electrostatic interactions. In the lateral view, we can appreciate the quality of the "average" plane obtained in different cases. For example, in the case of the G-C pair we can see that both bases have the same plane and do not show deviations from the average plane, as it was expected from a Watson–Crick base pair; however, for the G-U wobble pair, we can see that the bases are not coplanar, but they deviate from the average plane in opposite directions and in similar extent, just as it was expected. The results are similar for the other two positions, so we can say that the *ABC′* plane works well as an average plane.

The radial MEP scan approach offers the possibility to choose the region that we want to analyze from a proper selection of an interval of θ, and therefore the possibility to characterize more precisely the more exposed sites of each groove according to the relevance in the interaction with the enzyme.

For each pair, we propose three possible *n*-tuples. One for each groove and one for both grooves at the same time. The chosen θ intervals covering each groove, are considered to include the most exposed sites for a possible electrostatic recognition mechanism; the minor groove *n*-tuple $\mathbf{V}_{\text{minor}}$ corresponds to the interval $50^\circ \leq \theta \leq 130^\circ$ and the major groove one $\mathbf{V}_{\text{major}}$ corresponds to $230^\circ \leq \theta \leq 310^\circ$. The third *n*-tuple $\mathbf{V}_{\text{total}}$, covers the MEP intervals of the two previous ones (see Eqs. (5)–(7)). Points in the intervals $(130^\circ, 230^\circ)$ and $(310^\circ, 50^\circ)$ were suppressed due to the extremely high potential values produced by the small distance between the circumference and the atoms and also due to the non-specific interactions that these atoms may establish with the enzyme.

$$\mathbf{V}_{\text{minor}} = (V_{50^\circ}, V_{51^\circ}, \ldots, V_{130^\circ}) \quad (5)$$

$$\mathbf{V}_{\text{major}} = (V_{230^\circ}, V_{231^\circ}, \ldots, V_{310^\circ}). \quad (6)$$

$$\mathbf{V}_{\text{total}} = (V_{50^\circ}, \ldots, V_{130^\circ}, V_{230^\circ}, \ldots, V_{310^\circ}), \quad (7)$$

2.4. Base pairs classification by MEP similarity

To calculate how different two base pairs are, we used the Euclidean distance (δ) between their corresponding *n*-tuples.

$$\delta(\mathbf{V}^A, \mathbf{V}^B) = \left[\sum_i^n (V_i^A - V_i^B)^2\right]^{1/2} \quad (8)$$

where V_i^A and V_i^B are the *i*-th components of the *n*-tuples representing base pairs *A* and *B*. This distance may be considered as a measure of the dissimilarity between the electrostatic "key" induced by each base pair. Accordingly, two equal "keys" with equal *n*-tuples will have $\delta = 0$.

In order to classify the base pairs according to their MEP *n*-tuples, we used the *k*-means method, which is a non-hierarchical clustering approach [37], through which objects are grouped according to their distance to another object or to a previously constituted cluster. As a result, similar objects are grouped in the same cluster. This analysis was performed using the distance values computed according to Eq. (8), using the three different *n*-tuples available for each base pair. Considering that for every base pair, we have its corresponding $\mathbf{V}_{\text{minor}}$, $\mathbf{V}_{\text{major}}$ and $\mathbf{V}_{\text{total}}$, we obtained three different classifications for each position.

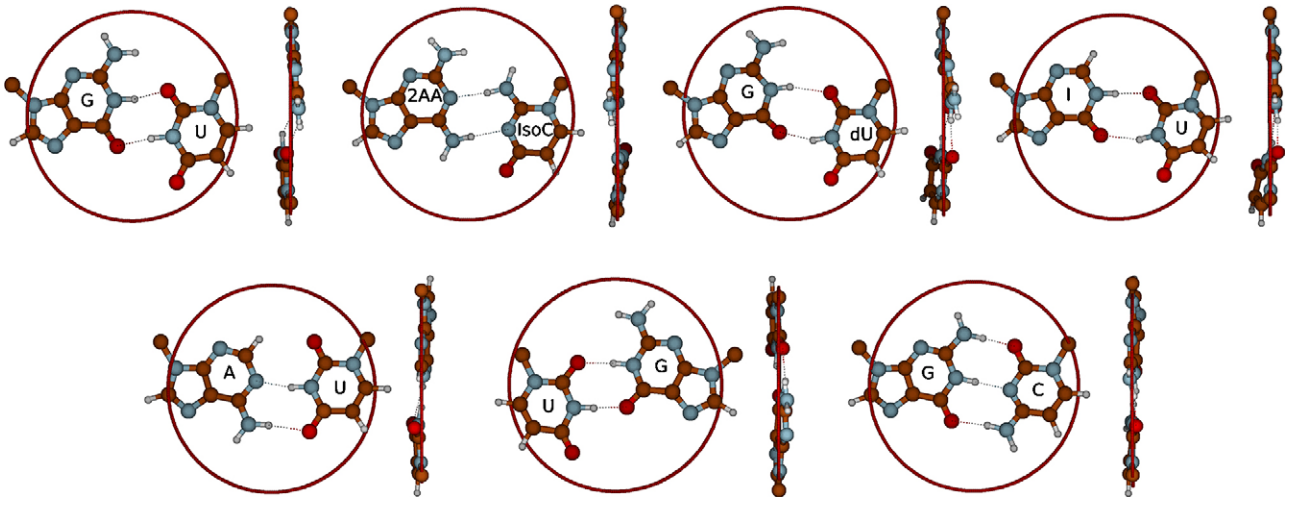

Fig. 5. Upper and lateral views for the base pairs considered in the positions 3–70 of $tRNA^{Ala}$ and their corresponding circumferences.

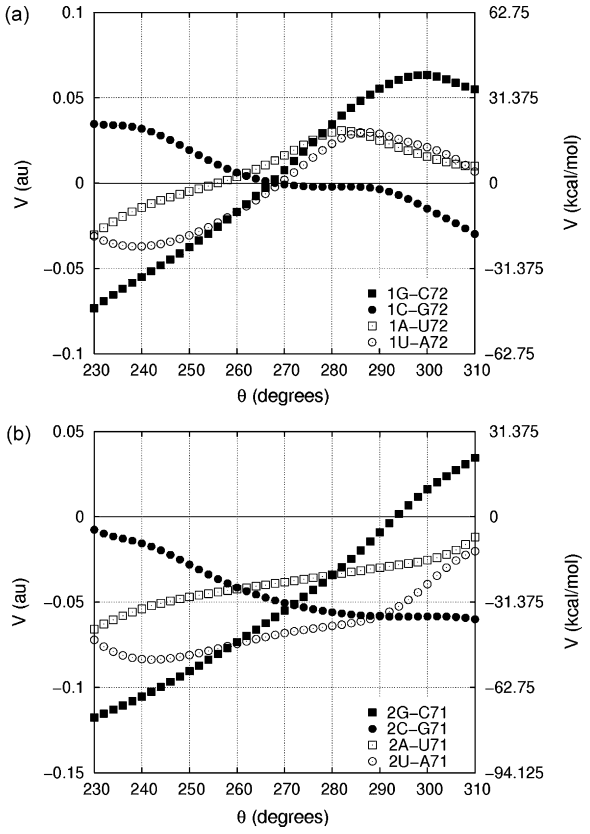

Fig. 6. V versus θ plots for the standard Watson–Crick base pairs in positions (a) 1–72 and (b) 2–71 of $tRNA^{Ala}$ acceptor stem. Both plots are for the major groove.

3. Results and discussion

3.1. Plotting the MEP values for $tRNA^{Ala}$ base pairs

3.1.1. The Watson–Crick base pairs transversions

The effect of base pair transversions for the standard Watson–Crick base pairs has been previously studied, particularly for the 1–72 and 2–71 positions [5,24], i.e. G-C → C-G and A-U → U-A. For both positions, the first transformation results in a total decrease of the activity (from $-\log K = 0$ to $-\log K = 4$), while for the second transversion the activity is almost unaffected (see Table 1). In Fig. 6 (a) and (b), we show the corresponding V versus θ plots for positions 1–72 and 2–71, respectively, regarding the major groove ($\mathbf{V}_{major}$) because this is the groove that the AlaRS should recognize in this position. In both figures, it is evident that the G-C and C-G base pairs have opposite MEP profiles in this groove, with an intersection around 270° and with a maximum difference of about 60 kcal/mol near to 230° and 310°. In the context of the electrostatic complementarity this means opposite and considerably different electrostatic "keys" that will cause a dramatic change in the complementarity and therefore in the recognition process. In contrast, the MEP profiles for A-U and U-A pairs are not opposite but rather similar in a considerable θ interval. These plots show that, in general, a base pair transversion does not necessarily cause a radical and opposite change in the MEP profile and consequently the effect in the activity depends on how different are the MEP profiles of the base pairs. From Fig. 6, it is clear why a G-C → C-G transversion is much more dramatic than the A-U → U-A one. The excellent agreement between these plots and the experimental results, provides significant evidence that contribute to the idea that the identity elements main role in the AlaRS-$tRNA^{Ala}$ is to guarantee electrostatic complementarity.

Table 2
Euclidean distances between major groove n-tuples and differences in activity for Watson–Crick base pair transversions

Pair 1[a]	$-\log K_1$	Pair 2	$-\log K_2$	$-\log K_2 + \log K_1$	$\delta(\mathbf{V}^1_{major}, \mathbf{V}^2_{major})$
Positions 1–72					
G-C	0.000	C-G	4.000	4.000	0.567
7DAG-C	−0.322	C-7DAG	2.201	2.523	0.389
I-C	0.174	C-I	2.620	2.446	0.452
G-4HC	0.340	4HC-G	2.620	2.280	0.490
U-2AP	1.260	2AP-U	1.886	0.626	0.140
A-U	2.398	U-A	2.398	0.000	0.138
Positions 2–71					
G-C	0.000	C-G	4.000	4.000	0.567
I-C	0.292	C-I	4.000	3.708	0.461
2AA-U	0.638	U-2AA	1.699	1.061	0.270
2AP-U	0.745	U-2AP	4.000	3.255	0.289
U-A	1.921	A-U	1.959	0.038	0.244

In order to extend this analysis to other Watson–Crick base pairs, we choose all the possible couples of pairs present in positions 1–72 and 2–71 that qualify as a base pair transversion. In Table 2, we show for each couple, the Euclidean distance between the corresponding major groove n-tuples and the difference in $-\log K$values. These numbers show that base pairs with large distances between MEP profiles have more distant activities, at the same time that base pairs with small distances present more similar activities. Despite the couple of pairs (2AP-U, U-2AP) in the 2–71 positions, these results are in agreement with the clear tendency observed in Fig. 6.

3.1.2. The 3G-U70 wobble pair

Twenty years ago Hou and Schimmel found the most critical identity element in the *E. coli* $tRNA^{Ala}$ and maybe the most studied one in the tRNA identity context: the 3G-U70 wobble pair [16]. This pair is responsible for much of the $tRNA^{Ala}$ identity and several efforts have been made in order to understand why this base pair is so important [16–21,25], some of them including X-rays and NMR studies to establish geometrical reasons for its relevance and function [38–41]. According to these studies, in order to be positively recognized by the enzyme, in the 3–70 positions must be an unpaired 2-amino group exposed to the minor groove from a purine in the position 3. Any wobble pair or an unpaired 2-amino group in any place of the minor groove is not enough.

In Fig. 7, we show the radial MEP scan plot for the minor groove of the base pairs studied in the positions 3–70. At first glance we can discriminate three kinds of MEP profiles: (i) those with a

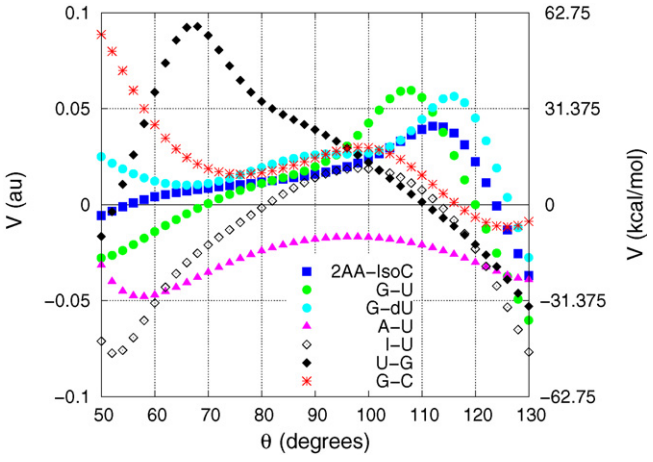

Fig. 7. V versus θ plot for the minor groove of the base pairs studied in positions 3–70.

marked maximum near 110°, (ii) the one with a marked maximum near 70° and (iii) those with not such maxima. If we confront these profiles with the experimental findings mentioned above, we can see a complete agreement. It can be seen that the three base pairs that present a maximum near 110° are the most active ones, and they are precisely the base pairs that have the unpaired 2-amino group in the purine in position 3 (see Figs. 2 and 5). Although the 3G-C70 pair also has a 2-amino group, this does not produce such a positive MEP.

The other relevant issue is the sensitivity of the enzyme to the position of this maximum. As in the case of the G-C → C-G transversion, due to the strong asymmetry of the 3G-U70 MEP profile, the 3U-G70 pair presents an opposite profile that is not recognized correctly by the AlaRS. This agrees with the work of Musier-Forsyth et al. [21], Beuning et al. [23] and Henderson et al. [42] where they affirm that it is not only the occurrence of an unpaired 2-amino group what matters, but also the position where this group is located. Since the hydrogen atom of the 2-amino group is almost at the center of the minor groove, it is not easy to imagine how could the enzyme make such a clear discrimination between G-U and U-G. However, in Fig. 7, it is evident that the position of this amino group is able to completely change the MEP profile and therefore the electrostatic fit between the enzyme and the $tRNA^{Ala}$.

3.2. Radial MEP scan for the ThrRS-$tRNA^{Thr}$ complex

As indicated by Ibba and Söll [28], AlaRS and ThrRS are class II synthetases that approach the tRNA acceptor stem in a similar way, i.e. they interact with both, minor and major grooves unlike other class II synthetases, that only interact with the major groove. Due to this similarity, we studied ThrRS-$tRNA^{Thr}$ interactions in order to test the capabilities of the radial scan of MEP to reveal specific behaviors in a similar system, one for which the experimental geometry complex is available. To reinforce how valuable is the information found in the radial MEP scan plots, we performed a detailed examination of the plots for the first two base pairs of $tRNA^{Thr}$ acceptor stem, trying to check whether the MEP produced by the base pairs near the enzyme's atoms is in accordance with an appropriate electrostatic complementarity.

It is already known that the wild-type base pairs, 1G-C72 and 2C-G71, establish hydrogen bonds in the minor groove with the enzyme, by means of the Tyr205 and Gly203, respectively (see Fig. 4b in Ref. [27]). In Fig. 8, we try to reproduce this view using the coordinates extracted from the ThrRS-$tRNA^{Thr}$ complex, but only showing each base pair with the corresponding interacting aminoacid lying in the minor groove. In both cases, we compute the corresponding circumference following the same methodology as for the $tRNA^{Ala}$ base pairs, and in green we show the points each 10° for two intervals: (i) $50° \leq \theta \leq 130°$ located in the minor grove and (ii) $230° \leq \theta \leq 310°$ located in the major groove. Two different perspectives are shown to illustrate the position of the interacting aminoacid relative to the base pair, and it is clear from this figure that oxygen atoms in the OH group of Tyr and in the CO group of Gly, lie really close to the green points, i.e. we can assume that these oxygen atoms are almost on the circumference. This gives us a good idea of which angle intervals are more critical for the

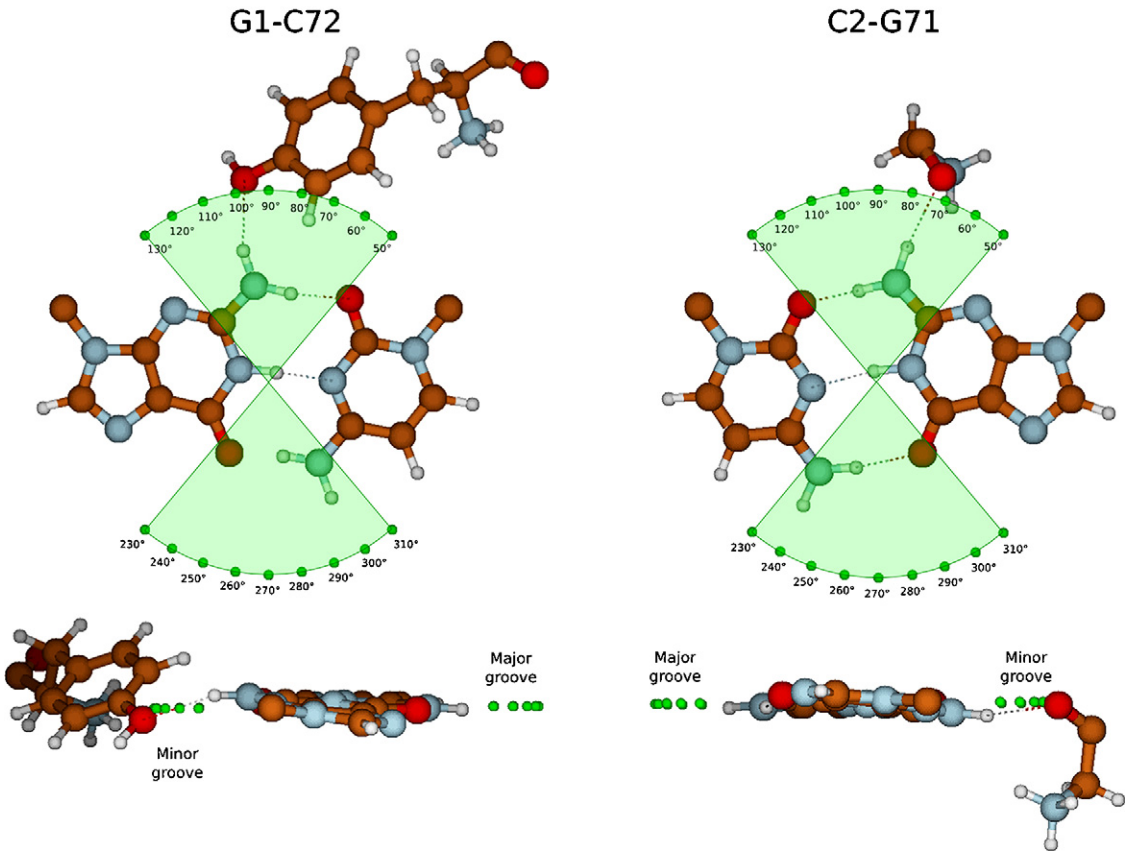

Fig. 8. Fragments of the ThrRS-$tRNA^{Thr}$ complex geometry where hydrogen bond interactions are established between the first two base pairs of the acceptor stem and the enzyme. Pair 1G-C72 interacts with the oxygen atom in the hydroxyl group of Tyr205 and pair 2C-G71 interacts with the oxygen in the carbonyl group of Gly203. The green points of the circumferences were obtained according to the introduced methodology.

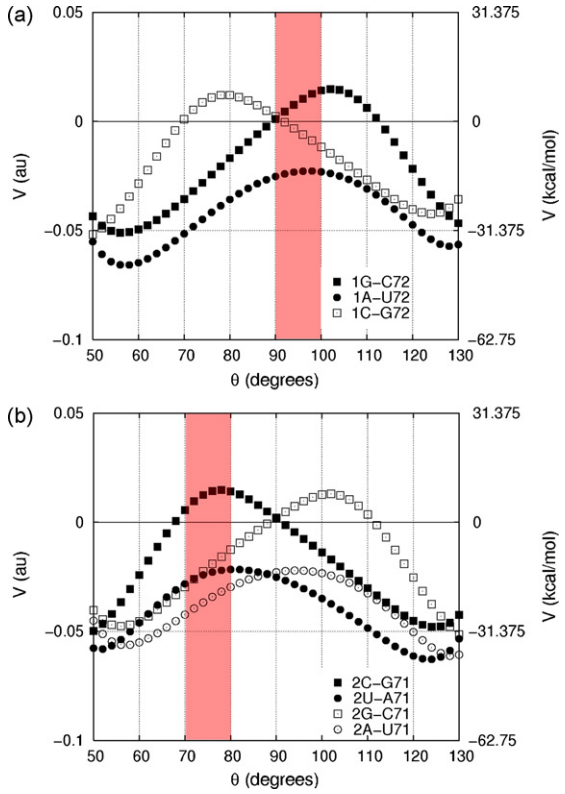

Fig. 9. V versus θ plots for the minor groove of the base pairs studied in positions (a) 1–72 and (b) 2–71 of $tRNA^{Thr}$ acceptor stem. The highlighted intervals correspond to the sites where ThrRS atoms interact with the base pair.

enzyme, and therefore it guide us to choose where to focus in the radial MEP scan plots. The chosen intervals are: $90^\circ < \theta < 100^\circ$ in the case of the 1–72 positions and $70^\circ < \theta < 80^\circ$ for the 2–71 positions (see Fig. 9).

Having selected specific sites of the base pairs minor groove, now we must examine the plots in detail. In Fig. 9(a) is the radial MEP scan plot for the base pairs considered in positions 1–72, regarding the minor groove vector. We can see that the MEP values for $90^\circ < \theta < 100^\circ$ behave accordingly with the aminoacylation activity. Only the G-C pair (which is the wild-type) has a positive potential in this interval which is complementary to the negative character of the oxygen atom, and therefore it shows the highest activity (lowest $-\log K$). Instead, the other two base pairs (C-G and A-U), exhibit negative potentials which should produce electrostatic repulsions in this critical point, and as a consequence the activity is reduced (see Table 1). In Fig. 9(b), the corresponding plot for the positions 2–71 is shown. In this case, the correlation between the MEP values for $70^\circ < \theta < 80^\circ$ and the activity is even better. Again, the only base pair exhibiting a positive potential in this interval is the wild-type (C-G); this potential allows to achieve complementarity with the oxygen atoms and therefore this pair also has the highest activity. Accordingly, the base pair with the lowest activity (A-U) shows the most negative potential, which should produce the strongest repulsion. The other base pairs (G-C and U-A) show similar potentials and also have similar activities, both being in between the extreme cases (see Table 1).

From the analysis presented above, we conclude that there is a good agreement between the MEP values in a restricted interval of the circumference and the activity for the $tRNA^{Thr}$, even more when such interval corresponds to a critical site in the ThrRS-$tRNA^{Thr}$ recognition mechanism. This results makes evident the usefulness of the radial MEP scan as a methodology to study protein–RNA interactions and therefore lead us to think that the AlaRS-$tRNA^{Ala}$ electrostatic complementarity should be governed by similar interactions.

3.3. MEP-activity relationship from the similarity classifications of $tRNA^{Ala}$ base pairs

In Table 3, we show the classifications obtained for each position in the $tRNA^{Ala}$ acceptor stem. According to the k-means method, we have to define a number of seeds to begin the analysis, and this number is going to define the number of final clusters. Thus, in every analysis we define three seeds: the base pair with the highest activity, one base pair with an intermediate activity and the base pair with the lowest activity. In Table 3, we use numbers to identify the cluster in which each base pair is

Table 3
Non-hierarchical clustering results obtained for the similarity classification of the $tRNA^{Ala}$ base pairs

Pair no.	Pairs 1–72 [a]				Pairs 2–71 [b]				Pairs 3–70 [c]			
	Cluster [d]				Cluster				Cluster			
	Ac. [e]	$\mathbf{V}_m$ [f]	$\mathbf{V}_M$ [g]	$\mathbf{V}_t$ [h]	Ac.	$\mathbf{V}_m$	$\mathbf{V}_M$	$\mathbf{V}_t$	Ac.	$\mathbf{V}_m$	$\mathbf{V}_M$	$\mathbf{V}_t$
1	0.000	2	1	1	0.000	1	1	1	0.000	1	1	1
2	−0.322	1	1	1	0.292	2	1	1	0.398	1	1	1
3	0.174	1	1	1	0.602	1	1	1	1.252	1	2	1
4	0.469	2	1	1	0.638	1	2	2	2.432	2	2	2
5	1.260	3	2	2	0.745	1	2	1	3.046	2	3	2
6	1.886	2	2	2	1.420	1	1	1	3.046	3	2	1
7	2.201	3	3	3	1.658	1	1	1	4.000	3	3	3
8	2.398	1	2	2	1.699	3	2	3				
9	2.398	3	2	2	1.921	2	2	2				
10	2.620	3	3	3	1.959	2	2	2				
11	2.620	3	3	3	4.000	3	2	3				
12	4.000	3	3	3	4.000	2	3	3				
13					4.000	3	3	3				

[a] Base pairs 1, 6 and 12 taken as seeds of clusters 1–3, respectively.
[b] Base pairs 1, 10 and 13 taken as seeds of clusters 1–3, respectively.
[c] Base pairs 1, 4 and 7 taken as seeds of clusters 1–3, respectively.
[d] Numbers indicate to which cluster belongs the base pair.
[e] $-\log K$activities.
[f] Classification obtained when the minor groove n-tuple was considered in the non-hierarchical clustering.
[g] Classification obtained when the major groove n-tuple was considered in the non-hierarchical clustering.
[h] Classification obtained when the total n-tuple was considered in the non-hierarchical clustering.

classified: high (1), intermediate (2) and low (3) activity. It is important to note that in the following analysis we use the terms *high*, *medium*, and *low* activities according to their positions in Table 1, without assuming a pre-established interval for each one of this categories.

3.3.1. Positions 1–72

For the 1–72 base pairs, it is possible to see that the classification produced by the major groove MEP, shows a better agreement with the aminoacylation activity than the one obtained from the minor groove *n*-tuples. In the major groove classification, the four pairs with the highest activity are classified in cluster 1 ($0.000 \leq -\log K \leq 0.469$), the pairs with intermediate activity are classified in cluster 2 ($1.260 \leq -\log K \leq 2.398$) and the three base pairs with the lowest activity are classified in cluster 3 ($2.620 \leq -\log K \leq 4.000$). Only one outlier was encountered, the pair 7, that is classified in the low activity cluster when it should be classified in the intermediate activity one. In an opposite way, the classification according to the minor groove does not show any clear partitions, except for the pairs 9–12 classified together in cluster 3 ($2.398 \leq -\log K \leq 4.000$). This results completely agree with the stereochemical preferences of the enzyme, which seems to approach this position from the major groove, i.e. if the AlaRS-$tRNA^{Ala}$ electrostatic interactions in this position are given in the major groove, and our hypothesis is correct, the similarity classification obtained from the corresponding *n*-tuples, is expected to reproduce a classification by activity. Additionally, we also notice that the $\mathbf{V}_{\text{total}}$ classification, is equal to the $\mathbf{V}_{\text{major}}$ one, possibly owing to the fact that differences in the minor groove *n*-tuples for these pairs are not large enough to obscure the more significant differences in the major groove *n*-tuples.

3.3.2. Positions 2–71

In the 2–71 positions, both classifications present outliers. In the minor groove classification, three outliers may be identified: pair 2, classified in the intermediate activity group, but it should be in the high activity group, pair 8 classified as low activity instead of intermediate or high, and pair 12 classified as intermediate instead of low. In the major groove classification there are two outliers: pairs 4 and 5, classified as intermediate instead of high; although, one also might say that the outliers are pairs 6 and 7, classified as high instead of intermediate. Therefore, it is clear that for this position the obtained classifications do not reflect the stereo chemical preferences of the AlaRS, as it was expected, i.e. that the major groove classification should be better than the minor groove one, as happened in the 1–72 positions. However, if we think about the enzyme's preferences in the 1–72 and 3–70 positions (major and minor grooves respectively), it would be logical that a transition point, where both grooves are equally important, was located in the 2–71 positions. If there were experimental evidence to assert that the change in the enzyme's priority owes to the internal curvature of the double helix, it would be acceptable that this transition point should exist and the better candidate would be the 2–71 base pairs, as the present results suggest. Nevertheless, this hypothesis can only be confirmed or refuted when the corresponding AlaRS-$tRNA^{Ala}$ complex geometry be established.

3.3.3. Positions 3–70

In accordance with the arguments given above, for positions 3–70 the classification obtained from the minor groove *n*-tuples is slightly superior than the major groove classification; something that also agrees with the preestablished preferences of the AlaRS. In the first classification, pairs 1–3 are found to be in cluster 1 (which are the only ones that show the maximum near 110° in Fig. 7), pairs 4 and 5 are in intermediate activity, and pairs 6 and 7 are classified as low active. While in the other two classifications there is one outlier (pair 6). For this position our results also agree with the experimental findings, reinforcing the idea that base pairs with similar MEP profiles should have similar activities.

4. Conclusions

We have developed a simple methodology to characterize and compare quantitatively the MEP in the minor and major grooves of RNA double helices, more precisely, the MEP in the vicinity of the more exposed atoms of the nitrogenated bases. The MEP, calculated on a circumference defined around each pair, is recorded as a *n*-tuple of MEP values, and this representation is suitable to be analyzed by graphical or statistical methods. The introduced methodology is general and is also applicable to DNA double helix systems where minor and/or major grooves need to be characterized electrostatically.

When the resulting *n*-tuples are plotted as V versus θ, the obtained graphics give a better understanding of the electrostatic patterns of the grooves. In the particular case of aaRS-tRNA interactions, and according to the electrostatic complementarity hypothesis, we may interpret this plots as a graphical description of the electrostatic "key" that must fit in the electrostatic "lock" of the enzyme. This is illustrated with the Watson–Crick base pairs transversion and some variants in 3–70 base pairs of the $tRNA^{Ala}$, in which close relations were found between the MEP profiles and the aminoacylation activity. More conclusive tendencies were found for the $tRNA^{Thr}$ cases, in which the X-ray crystal structure of the complex let us to corroborate the usefulness of the proposed methodology when studying how the aaRS-tRNA recognition is affected by changes in the identity elements of a tRNA. These results are a strong evidence that corroborates that the main role of the identity elements in the recognition process, is to maintain an appropriate electrostatic "key" to allow a good electrostatic complementarity.

In addition, when the *n*-tuples representing the MEP in the minor and major grooves were analyzed by means of statistical tools, as clustering, classifications by similarity were obtained. Here, we showed a non-hierarchical clustering performed for the set of $tRNA^{Ala}$ base pairs, and a good correlation with the aminoacylation activity was found, i.e. base pairs classified in the same group have similar activities. Furthermore, we found that the stereochemical preferences of the enzyme by a particular groove, previously deduced by experimental techniques, are reflected in the obtained classifications.

Acknowledgments

We acknowledge Prof. María Nagan at Truman State University for providing the nuclear geometries of molecules to study the third base pair of the $tRNA^{Ala}$. This work was supported by the Instituto Colombiano para el Desarrollo de la Ciencia y la Tecnología, Francisco Jos de Caldas—COLCIENCIAS.

References

[1] C.S. Francklyn, P. Schimmel, Synthetic RNA molecules as substrates for enzymes that act on tRNAs and tRNA-like molecules, Chem. Rev. (1990) 1327–1342.
[2] R. Giegé, M. Sissler, C. Florentz, Universal rules and idiosyncratic features in tRNA identity, Nucleic Acids Res. 26 (1998) 5017–5035.
[3] D. Tworowski, M. Safro, The long-range electrostatic interactions control tRNA-aminoacyl-tRNA synthetase complex formation, Protein Sci. 12 (2003) 1247–1251.
[4] D. Tworowski, A.V. Feldman, M.G. Safro, Electrostatic potential of aminoacyl tRNA synthetase navigates tRNA on its pathway to the binding site, J. Mol. Biol. 350 (2005) 866–882.

[5] P.J. Beuning, M.C. Nagan, C.J. Cramer, K. Musier-Forsyth, J.-L. Gelpi, D. Bashford, Efficient aminoacylation of the $tRNA^{Ala}$ acceptor stem: dependence on the 2:71 base pair, RNA 8 (2002) 659–670.
[6] G. Náray-Szabó, Quantum chemical calculation of the enzime-ligand interaction energy for trypsin inhibition by benzamidines, J. Am. Chem. Soc. 106 (1984) 4584–4589.
[7] P. Nagy, G. Náray-Szabó, Electrostatic complementarity between the catalytic triad and the protein environment in serine proteinases, J. Mol. Struct. THEOCHEM. 123 (1985) 413–419.
[8] G. Náray-Szabó, Electrostatic complementarity in molecular associations, J. Mol. Graph. 7 (1989) 76–81.
[9] G. Náray-Szabó, Analysis of molecular recognition: steric electrostatic and hydrophobic complementarity, J. Mol. Recognit. 6 (1993) 205–210.
[10] L. Gráf, L. Ágnes Jancsó, G. Szilágyi, K. Hegyi, G. Pintér, J. Náray-Szabó, K. Hepp, W.J. Medzihradszky, Rutter, Electrostatic complementarity within the substrate-binding pocket of trypsin, Proc. Natl. Acad. Sci. U.S.A. 85 (1988) 4961–4965.
[11] T. Gérczei, B. Asbóth, G. Náray-Szabó, Conservative electrostatic potential patterns at enzyme active sites: the anion–cation–anion triad, J. Chem. Inf. Comput. Sci. 39 (1999) 310–315.
[12] H. Nakajima, O. Kikuchi, Analysis of electrostatic and hydrophobic complementarities between trypsin and *Cucurbita maxima* trypsin inhibitor I using molecular electrostatic potential, J. Mol. Struct. THEOCHEM. 365 (1996) 39–45.
[13] C.A. Del Carpio, Y. Takahashi, S.-I. Sasaki, Automatic identification and manipulation of receptor sites in proteins. 2. electrostatic complementarity analysis for the evaluation and selection of candidate ligand receptor sites, J. Chem. Inf. Comput. Sci. 33 (1993) 769–775.
[14] A.J. McCoy, V.C. Epa, P.M. Colman, Electrostatic complementarity at protein/protein interfaces, J. Mol. Biol. 268 (1997) 570–584.
[15] G. Náray-Szabó, Quantitative estimation of electrostatic complementarity, Match Commun. Math Co. 44 (2001) 297–304.
[16] Y.-M. Hou, P. Schimmel, A simple structural feature is a major determinant of the identity of a transfer RNA, Nature 333 (1988) 140–145.
[17] W.H. McClain, K. Foss, Changing the identity of a tRNA by introducing a G · U wobble pair near the 3′ acceptor end, Science 240 (1988), 793–793.
[18] W.H. McClain, Y. Min Chen, K. Foss, J. Schneider, Association of transfer RNA acceptor identity with a helical irregularity, Science 242 (1988) 1681–1684.
[19] K. Musier-Forsyth, N. Usman, S. Scaringe, J. Doudna, R. Green, P. Schimmel, Specificity for aminoacylation of an RNA helix: an unpaired, exocyclic amino group in the minor groove, Science 253 (1991) 784–786.
[20] K. Gabriel, J. Schneider, W.H. McClain, Functional evidence for indirect recognition of G · U in $tRNA^{Ala}$ by alanyl-tRNA-synthetase, Science 271 (1996) 195–197.
[21] K. Musier-Forsyth, J.-P. Shi, B. Henderson, R. Bald, J.P. Fürste, V.A. Erdmann, P. Schimmel, Base-analog-induced aminoacylation of an RNA helix by a tRNA synthetase, J. Am. Chem. Soc. 117 (1995) 7253–7254.
[22] L. Hongjian, L.-P. Yap, K. Musier-Forsyth, Single atomic group in RNA helix needed for positive and negative tRNA synthetase discrimination, J. Am. Chem. Soc. 118 (1996) 2523–2524.
[23] P. Beuning, F. Yang, P. Schimmel, K. Musier-Forsyth, Specific atomic groups and RNA helix geometry in acceptor stem recognition by a tRNA synthetase, Proc. Natl. Acad. Sci. U.S.A. 94 (1997) 10150–10154.
[24] P.J. Beuning, M. Gulotta, K. Musier-Forsyth, Atomic group mutagenesis reveals major groove fine interactions of tRNA synthetase with an RNA helix, J. Am. Chem. Soc. 119 (1997) 8397–8402.
[25] M.C. Nagan, S.S. Kerimo, K. Musier-Forsyth, C.J. Cramer, Wild-type RNA $microhelix^{Ala}$ and 3:70 variants: molecular dynamics analysis of local helical structure and tightly bound water, J. Am. Chem. Soc. 121 (1999) 7310–7317.
[26] T. Hasegawa, M. Miyano, H. Himeno, Y. Sano, K. Kimura, M. Shimizu, Identity determinants of *E. coli* threonine tRNA, Biochem. Biophys. Res. Commun. 184 (1992) 478–484.
[27] R. Sankaranarayanan, A.-C. Dock-Bregeon, P. Romby, J. Caillet, M. Springer, B. Rees, C. Ehresmann, B. Ehresmann, D. Moras, The structure of threonyl-tRNA synthetase-tRNAThr complex enlightens its repressor activity and reveals an essential zinc ion in the active site, Cell 97 (1999) 371–381.
[28] M. Ibba, D. Söll, Aminoacyl-tRNA synthesis, Annu. Rev. Biochem. 69 (2000) 617–650.
[29] K. Musier-Forsyth, S. Scaringe, N. Usman, P. Schimmel, Enzymatic aminoacylation of single-stranded RNA with an RNA cofactor, Proc. Natl. Acad. Sci. U.S.A. 88 (1991) 209–213.
[30] W.D. Cornell, P. Cieplak, C.I. Bayly, I.R. Gould, K.M. Merz, D.M. Ferguson, D.C. Spellmeyer, T. Fox, J.W. Caldwell, P.A. Kollman, A second generation force field for the simulation of proteins, nucleic acids and organic molecules, J. Am. Chem. Soc. 117 (1995) 5179–5197.
[31] http://www.rcsb.org/pdb/explore/explore.do?structureid=1qf6 (accessed on February 25, 2008).
[32] G.A. Arteca, A. Hernández-Laguna, J.J. Rández, Y.G. Smeyers, P. Mezey, A topological analysis of molecular electrostatic potential on van der Waals surfaces for histamine and 4-substituted derivatives as H_2-receptor agonists, J. Comput. Chem. 12 (1991) 705–716.
[33] R.M. Marín, N.F. Aguirre, E.E. Daza, Graph theoretical similarity approach to compare molecular electrostatic potentials, J. Chem. Inf. Model. 48 (2007) 109–118.
[34] M. Daune, Molecular Biophysics Structures in Motion, first ed., Oxford University Press, 1993.
[35] N.B. Leontis, J. Stombaugh, E. Westhof, The non-Watson–Crick base pairs and their associated isostericity matrices, Nucleic Acids Res. 30 (2002) 3497–3531.
[36] M.J. Frisch, Gaussian 98 Rev. A 11, Gaussian Inc., Pittsburgh, PA, 2001.
[37] R.A. Johnson, D.W. Wichern, Applied Multivariate Statistical Analysis, fifth ed., Prentice Hall, Upper Saddle River, New Jersey 07458, 2002.
[38] S. Limmer, B. Reif, G. Ott, L. Arnold, M. Sprinzl, NMR evidence for helix geometry modifications by a G-U wobble base pair in the acceptor arm of *E. coli* $tRNA^{Ala}$, FEBS Lett. 385 (1996) 15–20.
[39] A. Ramos, G. Varani, Structure of the acceptor stem of *Escherichia coli* $tRNA^{Ala}$: role of the G3 · U70 base pair in synthetase recognition, Nucleic Acids Res. 25 (1997) 2083–2090.
[40] M. Vogtherr, H. Schübel, S. Limmer, Structural and dynamic helix geometry alterations induced by mismatch base pairs in double-helical RNA, FEBS Lett. 429 (1998) 21–26.
[41] U. Mueller, H. Schübel, M. Sprinzl, U. Heinemann, Crystal structure of acceptor stem of $tRNA^{Ala}$ from *Escherichia coli* shows unique G · U wobble base pair at 1.16 Å resolution, RNA 5 (1999) 670–677.
[42] B.S. Henderson, P. Beuning, J.-P. Shi, R. Bald, J.P. Fürste, V.A. Erdmann, K. Musier-Forsyth, P. Schimmel, Subtle functional interactions in the RNA minor groove at a nonessential base pair, J. Am. Chem. Soc. 120 (1998) 9110–9111.